ACS NANO

www.acsnano.org

ARTICLE

Triggering Gaussian-to-Exponential Transition of Displacement Distribution in Polymer Nanocomposites *via* Adsorption-Induced Trapping

Ming Hu,[‖] Hongbo Chen,[‖] Hongru Wang, Stanislav Burov, Eli Barkai, and Dapeng Wang*

Cite This: *ACS Nano* 2023, 17, 21708–21718

Read Online

ACCESS | Metrics & More | Article Recommendations | Supporting Information

ABSTRACT: **In many disordered systems, the diffusion of classical particles is described by a displacement distribution $P(x, t)$ that displays exponential tails instead of Gaussian statistics expected for Brownian motion. However, the experimental demonstration of control of this behavior by increasing the disorder strength has remained challenging. In this work, we explore the Gaussian-to-exponential transition by using diffusion of poly(ethylene glycol) (PEG) in attractive nanoparticle−polymer mixtures and controlling the volume fraction of the nanoparticles. In this work, we find "knobs", namely nanoparticle concentration and interaction, which enable the change in the shape of $P(x,t)$ in a well-defined way. The Gaussian-to-exponential transition is consistent with a modified large deviation approach for a continuous time random walk and also with Monte Carlo simulations involving a microscopic model of polymer trapping *via* reversible adsorption to the nanoparticle surface. Our work bears significance in unraveling the fundamental physics behind the exponential decay of the displacement distribution at the tails, which is commonly observed in soft materials and nanomaterials.**

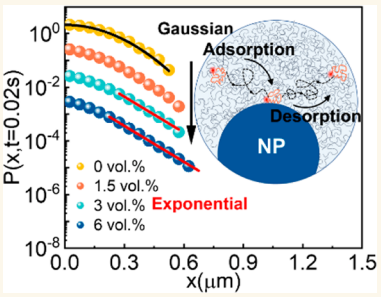

KEYWORDS: *polymer diffusion, single-molecule tracking, continuous time random walk, exponential decay, polymer nanocomposites*

Einstein's theory of Brownian diffusion predicts that the displacement of a group of particles follows a Gaussian distribution, with the variance increasing linearly with time t.[1] However, in materials close to the glass and jamming transitions, exponential decay of $P(x, t)$ was observed.[2−4] Interestingly, the exponential decay of $P(x, t)$ was found in a wide variety of scenarios: desorption-mediated diffusion on solid−liquid interfaces,[5−8] Brownian motion in polymer solutions,[9,10] cellular environments,[11−13] active systems,[14] heterogeneously crowded and confined media,[15−17] and even the fluctuations of price−time series in the stock market.[18] Well-designed theories and simulations have been put forward to rationalize the appearance of the exponential tail, such as the "diffusing diffusivity" model,[19−25] superstatistical approaches,[26−28] the quenched trap model,[29−31] and the hitchhiker-type model.[32−34] More recently, the large deviation theory was applied to a continuous-time random walk (CTRW) model to describe the exponential decay of $P(x, t)$. A CTRW process comprises intermittent switching between random immobile trapping periods and jumping steps.[35−38] The trapping duration dictates the random fluctuations in the number of displacement steps at a given t, which leads to an exponential decay of $P(x, t)$.[4,39,40]

The emergence of exponential $P(x, t)$ is significant, because it necessitates the consideration of theories based on hypothetical Gaussian diffusion. For instance, the Gaussian search is ten times slower than a molecular search with exponentially decaying groups.[41,42] More specifically, in many experimental systems where the exponential decay of $P(x, t)$ is observed, there is evidence of caging dynamics involving hops between different trapping sites.[10,43,44] The CTRW model is widely used to describe such behavior. Interestingly, the shape of $P(x, t)$ exhibits similarity across different systems, where the center follows a Gaussian distribution while the tail decays exponentially as $P(x, t) \sim \exp[-|x|/\lambda(t)]$.[9,45] With increasing time, Gaussian statistics become more dominant, as the central part of the spreading group is typically described by the central

Received: July 25, 2023
Accepted: October 13, 2023
Published: October 25, 2023

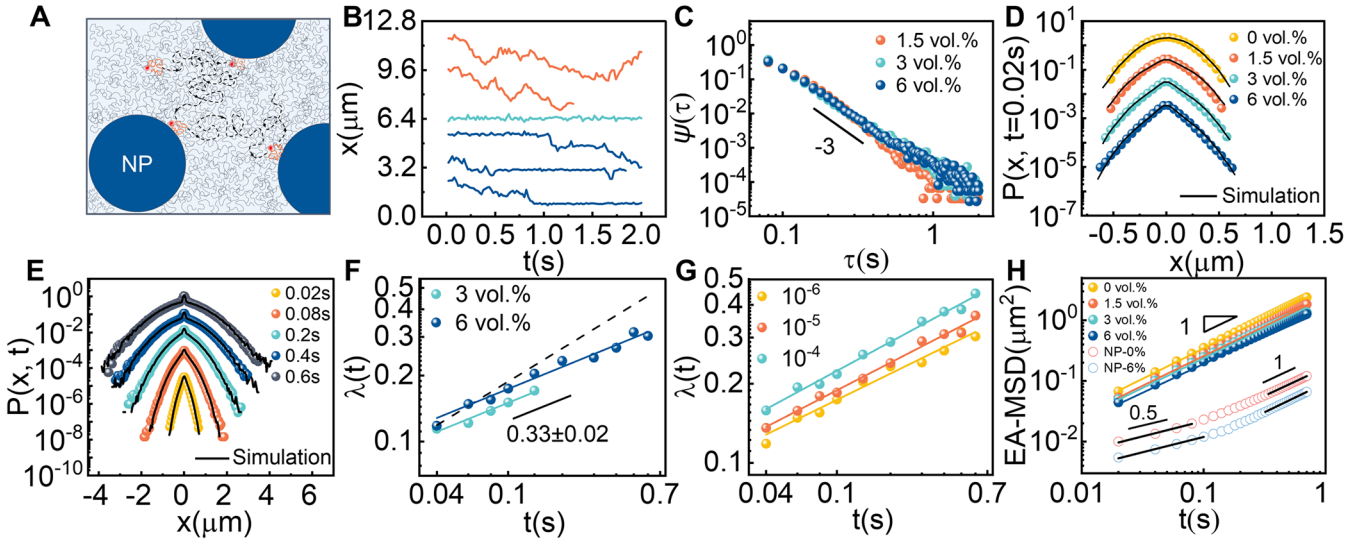

Figure 1. Diffusion in PEG-nanoparticle mixtures. (A) Schematic representation of dye-labeled PEG (red) diffusing in a PEG-nanoparticle (NP) mixture. (B) Lateral positions of representative trajectories of dye-labeled PEG at nanoparticle volume fraction Φ = 6 vol %. (C) Distributions of immobile times for polymer trajectories at different Φ. The solid line illustrates the power-law decay $\psi(\tau) \sim \tau^{-3}$. (D) $P(x, t)$ for the tracer polymer in mixtures with different Φ values at t = 0.02 s. Curves for data with Φ = 3 and 6 vol % exhibit exponential tails. (E) $P(x, t)$ for data of Φ = 6 vol % at different t values as annotated. The symbols in (D) and (E) denote experimental data, and the solid black lines indicate the simulation results. To guide the eye, the curves in (D) and (E) were vertically shifted. (F) Length scale $\lambda(t)$ for $P(x, t)$ of Φ = 3 and 6 vol % *vs* t. The dashed line denotes diffusive scaling, $\lambda(t) \sim t^{0.5}$. (G) Length scale $\lambda(t)$ *vs* t for minimum probability $P_{min} = 10^{-6}$, 10^{-5}, and 10^{-4} of Φ = 6 vol %. The lines represent power-law fits to the form $\lambda(t) \sim t^{\alpha}$. The exponent α can be considered as a constant within experimental uncertainty. (H) Ensemble-averaged mean squared displacement (EA-MSD) *vs* lag time t for PEG (filled spheres) with different Φ and fluorescent silica nanoparticles (hollow spheres) at Φ = 0 and 6 vol %. All measurements were performed in 20 vol % PEG solution. EA-MSDs grow linearly with t for PEG over studied t while nanoparticles exhibit normal diffusion for t > 0.08 s. The lines represent power-law fits to the form EA-MSD = $4Dt^{\xi}$.

limit theorem. A key question addressed in this article is how to control the exponential tail at a given time.

A second dilemma revolves around physical interpretation of the length scale $\lambda(t)$. This issue has sparked debate, with three different perspectives on the matter. In certain experiments, the length scale $\lambda(t)$ exhibits diffusive scaling of $\lambda(t) \sim t^{\alpha=1/2}$, where α is the scaling exponent. This behavior is observed in the diffusion of colloidal beads in entangled actin suspensions and on phospholipid bilayer tubes.[14,46] Moreover, other studies revealed a different scaling behavior with $\lambda(t) \sim t^{1/3}$.[13,47−50] Miotto *et al.* used molecular dynamics simulations to reveal $\lambda(t) \sim t^{1/d}$, where d is the dimension;[47] they also found the failure of using CTRW to describe the power-law dependence of $\lambda(t)$. Their claim concerning CTRW is based on an asymptotic expression that in turn is valid in a very long time limit. This links to a third viewpoint that argues against the existence of a typical length scale $\lambda(t)$,[48] attributing the results as mentioned above to finite-time effects and insufficient data.[51−53] Our goal is to clarify these issues both experimentally and theoretically.

In this work, we used single-molecule fluorescence tracking to study the diffusion of fluorescently labeled poly(ethylene glycol) (PEG) in mixtures containing nanoparticles and nonfluorescent PEG. PEG can reversibly adsorb on the nanoparticle surface when pH < 7 because of hydrogen bonds between the ether group of PEG and the hydroxyl group on the nanoparticle surface.[6,54] The adsorption-induced trapping triggers a CTRW-like motion, leading to exponential tails of the group of particles under conditions that we will clarify. In such a model system, we can control the CTRW dynamics, particularly the trapping time distribution and the proportion of CTRW-like trajectories among all diffusive trajectories, and see the pronounced effect on the exponential tails that result from adsorption-induced trapping.[55] We show that one can find a constant exponent α = 1/3 within experimentally accessible time and length scales. Theoretically, when simulating the dynamics with a CTRW approach, we show how this nontrivial exponent α = 1/3 emerges on short-time scales, further indicating the importance of this unexpected exponent.[52,53]

RESULTS AND DISCUSSION

Single-Molecule Tracking Results. This study performed all measurements in 20 vol % PEG solution with various nanoparticle volume fractions Φ. Figure 1B shows the lateral position of representative trajectories in a mixture with the volume fraction of nanoparticles Φ = 6 vol % as a function of time. Many mobile trajectories randomly switched between periods of immobilization and mobility, consistent with what was predicted by the CTRW theory (Figure 1B). We introduce a threshold distance (0.2 μm) to distinguish the immobile phase from the steps with a short displacement. We determine an immobile period in which the displacements of at least three consecutive steps are less than the threshold distance. Therefore, an immobile period shorter than 0.06 s (3 times the acquisition time) is inaccessible. The immobile time distribution $\psi(\tau)$ can be approximated as the power-law decay $\psi(\tau) \sim \tau^{-3}$ (Figure 1C). The immobile time distribution could be extrapolated to even smaller time scales, signifying that at any τ, the diffusion step could contain multiple switches between mobility (corresponding to the hop) and immobilization. The CTRW theory predicts Fickian diffusion in the EA-MSD sense, as we observed (Figure 1H). We further calculated

https://doi.org/10.1021/acsnano.3c06897
ACS Nano 2023, 17, 21708−21718

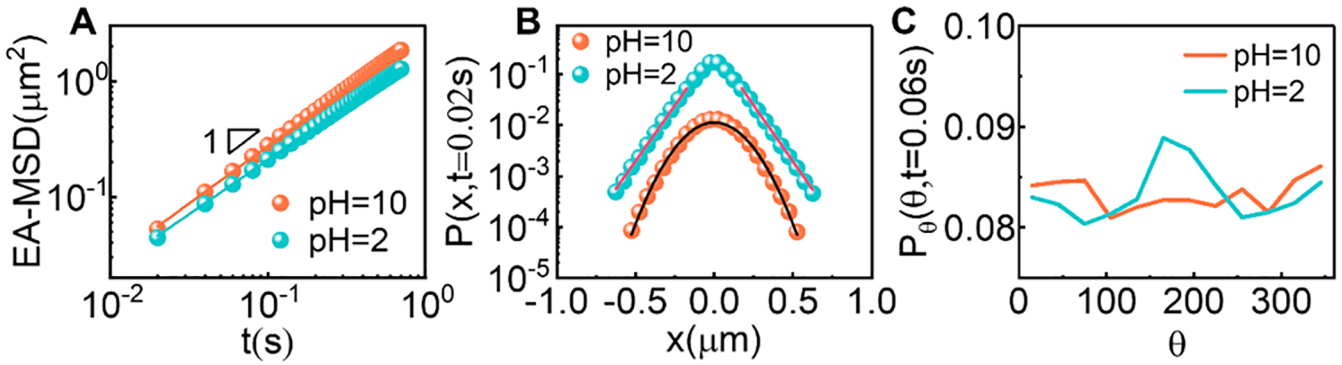

Figure 2. Control of exponential tails by varying pH. (A) EA-MSD and (B) $P(x, 0.02\ s)$ of the dye-labeled PEG at Φ = 6 vol % for pH = 2 and 10, respectively. The lines in (A) represent the fits to EA-MSD = $4Dt$. In (B), the black line is fitted by the Gaussian function, and the red lines represent the fits to the exponential tail as $\exp(-|x|/0.098)$ within the range $|x| > 0.15\ \mu m$. The data of pH = 10 in (B) were vertically shifted downward. (C) Relative angle distributions $P_\theta(\theta, t = 0.06\ s)$ in a 6 vol % mixture at pH = 2 and 10, for t = 0.06 s.

the displacement distribution in terms of the self-part of the van Hove correlation function $P(x, t)$.[56] This distribution represents the probability that a walker has moved a distance x in one dimension during time t. $P(x, t)$ of the polymer in entangled PEG solution is Gaussian at all studied t. With increasing Φ, the tails become non-Gaussian, and a small cusp at $x = 0\ \mu m$ emerges (Figure 1E and Figure S17). $P(x, t)$ was observed to decay linearly on a semilog plot for Φ = 3 and 6 vol % when $t < 0.08$ s (Figure 1D) and can be expressed as $P(x, t) \propto \exp[-|x|/\lambda(t)]$. The exponential decay was confirmed by implementing a nonparametric Kolmogorov–Smirnov test (Supporting Information). The exponential decay at the tail can smoothly revert to Gaussian with an increase in t (Figure 1E).

Interestingly, the appearance of exponential decay and its transition to Gaussian did not influence the linearity of EA-MSD (Figure 1H). The relaxation time t_d of entangled polymers is 0.57 ms, which is discussed below. Therefore, the observed polymer diffusion is in their viscous regime. Because the EA-MSD of polymers is linear, the diffusion coefficient D was obtained *via* fitting $D = \langle \Delta r^2 \rangle / 4t$, yielding values of 0.85, 0.66, 0.51, and 0.44 $\mu m^2/s$ for Φ = 0, 1.5, 3, 6 vol %, respectively. This trend can be attributed to the increase of viscosity.[57−61] Moreover, we measured the fluorescent nanoparticle diffusion in 20 vol % entangled polymer solution (Figure 1H). The nanoparticle exhibits a subdiffusion-to-diffusion transition that occurs at about 0.08 s. This time scale is longer than t_d (0.57 ms, described below) and can be attributed to topological constraints[62] and localization errors[63] that overestimate displacements due to the ultraslow nanoparticle diffusion. This phenomenon has been previously reported in similar systems.[63] The nanoparticle diffusion coefficient (0.042 $\mu m^2/s$) is much slower than the polymer diffusion. Therefore, the nanoparticle could be considered immobile on the time scale of polymer diffusion that was observed and analyzed in the present study.

Interestingly, we found $\lambda(t) \sim t^\alpha$ with $\alpha = 1/3$ for a representative case of Φ = 3 and 6 vol % (Figure 1F), which is phenomenologically consistent with those in multiple experimental systems.[13,47,48] Note that this value of α was scrutinized since α may depend on the length and time scales over which the fitting is made.[53] Therefore, we set up a minimum probability (P_{min}) of finding a particle at x at time t (see Figure 3C for an illustration) and recalculated $\lambda(t)$ as a function of t (Figure 1G). Yet, a constant α is found within experimental uncertainty with the increase of P_{min}. Importantly, varying the fitting range even further, in most systems for $P(x, t)$ with exponential tails, seems very challenging experimentally, and we conclude that within a reasonable time window, α is a constant and $\lambda(t) \sim t^{1/3}$.

We next studied the physical origin of immobilization by distinguishing between steric hindrance as proposed previously due to the high density of nanoparticles and hydrogen-bonding interactions.[64−66] To study whether the interaction leads to immobilization, we comparatively analyzed the diffusion statistics in mixtures with 6 vol % nanoparticles at pH = 2 and 10 because hydrogen bond dissociation occurs for pH > 8.[6] When the attractive interaction is eliminated, the EA-MSD scales linearly with t while $P(x, t)$ is Gaussian over the studied range of t (Figure 2A,B). At intermediate pH = 6, we found that the trajectories are Fickian and $P(x, t)$ deviates from Gaussian (Figure S16). Combined, the exponential tails of $P(x, t)$ are hypothesized to originate from the polymer–nanoparticle interaction that leads to adsorption on the nanoparticle surface with a wide span of random immobilized times between excursions through the bulk polymer medium (Figure 1A).[67] A step at any given t can be subdivided into many steps that were switched between immobilization and mobility. This physical scenario is supported by the relative angle analysis (Figure 2C and Figure S13, Supporting Information),[68] which measures the direction distribution between successive steps. We observe a peak at $\theta = 180°$ that denotes trapping events,[68] which are crucial ingredients for CTRW. Therefore, this supports the consistency of the experimental data and the CTRW model.

When polymers are dispersed in a matrix with a high concentration of nanoparticles, *e.g.*, Φ = 6 vol %, the presence of nanoparticles could limit exploratory space. As a result, the D values of polymers may decrease. Composto *et al.* demonstrated that the normalized diffusion coefficient of polymers can be collapsed onto a master curve by plotting it against a confinement parameter ($ID/2R_g$), where R_g represents the radius of gyration of the polymer and ID is interparticle distance.[69] The decrease in D can be attributed to the excluded volume effect.[70] In the case of pH = 10 where the adsorption does not take place and polymer–nanoparticle interaction is negligible, we did observe a Fickian and Gaussian diffusion with a decrease in D relative to that in a pure polymer system, which is consistent with previous studies.[69] In the case of pH = 2, the polymers tend to adsorb onto the surface of the

https://doi.org/10.1021/acsnano.3c06897
ACS Nano 2023, 17, 21708−21718

nanoparticles. This adsorption-induced trapping leads to the emergence of an exponential tail in the distribution of $P(x, t)$, which sets it apart from confined diffusion.

Kinetic Monte Carlo Simulation Results. To quantitatively test this hypothesis, we modeled the polymer diffusion using kinetic Monte Carlo simulations by integrating the adsorption process into the minimal model framework consistent with a mobile−immobile model.[71] The generalized random walk simulation was performed on a two-dimensional lattice containing uniformly distributed impermeable obstacles, with areal fractions of 1.5, 3, and 5% to mimic the experimental systems (Figure S5A, Supporting Information). On the time scale of polymer diffusion, the obstacles are approximately immobile. We fixed the obstacles to the lattice to simplify the polymer diffusion model. The polymer walker performed a random walk in an area that was not occupied by obstacles. When a walker comes into a lattice adjacent to an obstacle, there is a probability P_i to be immobilized with the duration that follows the experimentally measured $\psi(\tau) \sim \tau^{-3}$ (Figure 1C).

The simulations were compared with the experimental observations. The simulation parameters were chosen to be similar to the experimentally measured values, including the diffusion coefficient of PEG in PEG-nanoparticle mixtures, the volume fraction of nanoparticles, the proportion of entirely immobile trajectories, and other parameters associated with experimental distributions of immobile times (Figure 1C and Table S2). Note that P_i is the only adjustable parameter in the simulation. By setting $P_i = 0.03$, the simulation is quite consistent with experimental observations; the shape of $P(x, t)$ changes from a Gaussian to an exponential decay with increasing t and Φ values (Figure 1D,E and Figure S5). Although this minimal model does not include system-specific effects,[72,73] we believe that the simulation using a simple phenomenological model includes the most necessary information to capture adsorption on a nanoparticle surface as the origin of the emergence of the exponential tail of $P(x, t)$.

To examine the accuracy of our analysis, we kept $P_i = 0$ while adjusting the diffusion coefficient of all or a fraction of the trajectories to fit the data. Unfortunately, manipulating the diffusion coefficient failed to provide good agreement with experimental data in all cases; *i.e.*, the simulations were not consistent with the behavior of $P(x, t)$ at different t and Φ. Thus, this testing highlights the importance of immobilizing polymers close to nanoparticle surfaces to maintain congruity between simulation and reality. Careful analysis of the simulated trajectories indicates that there are trajectories that show pure diffusive behavior because of a very small P_i. As such, it is necessary to employ a mixture of models to describe the diffusion of polymers in the system, which includes both pure diffusion and transitions to/from nanoparticles.

Modified Large Deviations Approach for a CTRW. The polymer diffusion behavior in our system was found to conform to the CTRW model. We used an analytical approach to set up the switch between moving steps and random immobile times.[39,40] In short, the probability density function $P_{\mathrm{CTRW}}(X, t)$ is subordinated to the spatial process for X by the temporal process for N *via*

$$P_{\mathrm{CTRW}}(X, t) = \sum_{N=0}^{\infty} \mathcal{P}_N(X) Q_t(N)$$

$$\mathcal{P}(X) \sim \exp\left[-N\left(\frac{|X|}{\delta N}\right)^{\beta}\right] \qquad |X| \to \infty \tag{1}$$

where $\mathcal{P}_N(X)$ is the probability density function (PDF) of finding the particle at position X after N steps as a subordination of large deviations, $Q_t(N)$ is the probability of observing N steps at time t, and δ is the standard deviation of $\mathcal{P}_N(X)$. For the CTRW, one can decompose the process into a discrete hop-process and temporal immobilization processes, an approach called subordination. When the distribution of immobile time τ between two steps $\psi(\tau)$ can be analyzed around zero, with the Taylor expansion $\psi(\tau) \underset{\tau \to 0}{\sim} \sum_{j=0}^{\infty} C_{A+j}\tau^{A+j}$, $Q_t(N)$ can be expressed as

$$Q_t(N) \underset{N \to \infty}{\sim} \frac{\{C_A \Gamma(A+1)^{1/(A+1)} t\}^{N(A+1)}}{\Gamma[N(A+1)+1]} \exp\left(\frac{C_{A+1}}{C_A} t\right) \tag{2}$$

where C_A and C_{A+1} are the corresponding parameters in Taylor expansion for an experimental $\psi(\tau)$. The particles perform random walks in the bulk solution in the system, so $\mathcal{P}_N(X)$ is Gaussian with $\beta = 2$.

$$\mathcal{P}_N(X) \simeq \frac{1}{\sqrt{2\pi\delta^2 N}} \exp\left[-N\left(\frac{|X|}{\delta N}\right)^2\right] \tag{3}$$

Then, we substitute eqs 2 and 3 in eq 1 and by the Stirling approximation $N! \simeq \sqrt{2\pi N}\left(\frac{N}{e}\right)^N$. The PDF is converted into

$$P_{\mathrm{CTRW}}(X, t) \sim \int_0^{\infty} \exp(-K(N, X, t))\, \mathrm{d}N/2\pi\delta N$$

$$K(N, X, t) = N\left(\frac{|X|}{\delta N}\right)^2 - \frac{C_{A+1}}{C_A} t - N(A+1) \left[\ln\left(\frac{C_A \Gamma(A+1)^{1/(A+1)} t}{N(A+1)}\right) + 1\right] \tag{4}$$

Because the decay of experimental $\psi(\tau)$ follows a power-law function, we used the simple form $\psi(\tau) = \frac{1}{\tau_0}\frac{k-1}{(1+\tau/\tau_0)^k}$ called Dagum distribution. The parameter $k = 3$ is obtained by calculating the slope of the power law on the log−log plot of the distribution of $\psi(\tau)$ (that is consistent with experimental observations, as shown in Figure 1C). Once k is known, the other parameter $\tau_0 = 0.0115$ is obtained by fitting the whole form of the Dagum distribution to the experimental plot. The Taylor expansion $\psi(\tau) = \frac{1}{0.0115}\frac{2}{(1+\tau/0.0115)^3}$ is given as follows:

$$\psi(\tau) \underset{\tau \to 0}{\sim} \sum_{j=0}^{\infty} C_{A+j}\tau^{A+j}$$

$$= \frac{2}{0.0115} + \frac{-6}{0.0115^2}\tau + \frac{\psi_0''}{2!}\tau^2 + \ldots + \frac{\psi_0^{(j)}}{j!}\tau^j \tag{5}$$

Keeping the leading terms of $Q_t(N)$ in the large N limit, we use $A = 0$, $C_0 = 173.913\ \mathrm{s}^{-1}$, and $C_1 = -45386.6\ \mathrm{s}^{-2}$, which were substituted into $K(N, X, t)$ in eq 4 to yield

https://doi.org/10.1021/acsnano.3c06897
ACS Nano 2023, 17, 21708−21718

$$K(N, X, t) = N\left[\frac{1}{\delta}\frac{|X|^2}{N}\right] - \frac{C_1}{C_0}t - N[\ln(C_0 t) - \ln N + 1] \quad (6)$$

Using the saddle point approximation, the integral for PDF is approximately evaluated by the minimum of $K(N, X, t)$, which is obtained at N^* that satisfies $dK(N, X, t)/dN|_{N=N^*} = 0$. After differentiation, N^* is given by the formula

$$N^* = (|X|/\delta)/W_0(X^2/C_0^2 t^2 \delta^2)^{1/2} \quad (7)$$

where $W_0(y)$ is the principal branch of a Lambert W function, $W(y)\exp[W(y)] = y$. Thus, the PDF in eq 4 is then estimated as

$$P_{CTRW}(X, t) \sim \exp(-K(N^*, X, t)) / (N^* \sqrt{2\pi\delta^2 K''(N^*, X, t)}) \quad (8)$$

where $K''(N^*, X, t) = \frac{1}{N^*} + \frac{X^2}{\delta^2}\frac{1}{N^{*3}}$. Using eq 7, we obtained the $P_{CTRW}(X, t)$ expression as follows:

$$P_{CTRW}(X, t) \sim \frac{\exp\left\{-t\left[\frac{|X|}{t\delta}\left(\sqrt{W_0\left(\frac{X^2}{C_0^2 t^2 \delta^2}\right)} - 1/\sqrt{W_0\left(\frac{X^2}{C_0^2 t^2 \delta^2}\right)}\right) - \frac{C_1}{C_0}\right]\right\}}{\sqrt{2\pi\delta|X|\left(\sqrt{W_0\left(\frac{X^2}{C_0^2 t^2 \delta^2}\right)} + 1/\sqrt{W_0\left(\frac{X^2}{C_0^2 t^2 \delta^2}\right)}\right)}} \quad (9)$$

Because the nanoparticles are sparsely distributed in the polymer solution, we introduced a component to account for trajectories exhibiting Brownian diffusion and not interacting with nanoparticles during the experimental tracking. This is because some trajectories do not show immobilization. The displacement distribution $P_G(X, t)$ of these Brownian trajectories must obey a Gaussian distribution:

$$P_G(X, t) = \frac{1}{\sqrt{2\pi(\delta^2/\tau_0)t}} \exp\left[\frac{-X^2}{2(\delta^2/\tau_0)t}\right] \quad (10)$$

Here, we assume the jump size (*i.e.*, excursion after desorption) δ relates to diffusivity D_G *via* $D_G = \delta^2/2\tau_0$. The total PDF is the superposition of a Brownian process and a CTRW process

$$\begin{aligned} P(X, t) &= fP_G(X, t) + (1 - f)\frac{1}{\mathcal{N}}P_{CTRW}(X, t) \\ &\simeq f\frac{1}{\sqrt{2\pi(\delta^2/\tau_0)t}} \exp\left[\frac{-X^2}{2(\delta^2/\tau_0)t}\right] + (1 - f)\frac{1}{\mathcal{N}} \exp(-K(N^*, X, t))/(N^*\sqrt{2\pi K''(N^*, X, t)}) \\ &\simeq f\frac{1}{\sqrt{2\pi(\delta^2/\tau_0)t}} \exp\left[\frac{-X^2}{2(\delta^2/\tau_0)t}\right] + (1 - f)\frac{1}{\mathcal{N}} \frac{\exp\left\{-t\left[\frac{|X|}{t\delta}\left(\sqrt{W_0\left(\frac{X^2}{C_0^2 t^2 \delta^2}\right)} - 1/\sqrt{W_0\left(\frac{X^2}{C_0^2 t^2 \delta^2}\right)}\right) - \frac{C_1}{C_0}\right]\right\}}{\sqrt{2\pi\delta|X|\left(\sqrt{W_0\left(\frac{X^2}{C_0^2 t^2 \delta^2}\right)} + 1/\sqrt{W_0\left(\frac{X^2}{C_0^2 t^2 \delta^2}\right)}\right)}} \end{aligned} \quad (11)$$

where δ^2 is the variance of a Gaussian function $G(X) = \frac{1}{\sqrt{2\pi\delta^2}}\exp\left(\frac{-X^2}{2\delta^2}\right)$. The limit $f = 0$ was studied previously.[40] f is the only fitting parameter that denotes the proportion of the free diffusive component. $\mathcal{N}$ is the normalization constant obtained from the integral of $P_{CTRW}(X, t)$ (eq 9)

$$\mathcal{N} = \int_{-\infty}^{\infty} \frac{\exp\left\{-t\left[\frac{|X|}{t\delta}\left(\sqrt{W_0\left(\frac{X^2}{C_0^2 t^2 \delta^2}\right)} - 1/\sqrt{W_0\left(\frac{X^2}{C_0^2 t^2 \delta^2}\right)}\right) - \frac{C_1}{C_0}\right]\right\}}{\sqrt{2\pi\delta|X|\left(\sqrt{W_0\left(\frac{X^2}{C_0^2 t^2 \delta^2}\right)} + 1/\sqrt{W_0\left(\frac{X^2}{C_0^2 t^2 \delta^2}\right)}\right)}} dX \quad (12)$$

The normalization is necessary because the theory does not work in the vicinity of $X \to 0$. More specifically, it does not include the probability of performing zero steps, *i.e.*, immobile particles.

The theoretical parameters were designed to be as similar as possible to the associated experimentally measured values (Table S3). δ values were obtained from EA-MSD at pH = 10 with different volume fractions of nanoparticles shown in Figure S8. Using the experimental parameters as inputs, with f being the only adjustable parameter (Table S3), this model can adequately reproduce the experimental data (Figure 3A,B). The Brownian process was dominant for Φ = 1.5 vol % (f = 0.87). Even though 77% of the trajectories executed the Brownian process, the tail of $P(x, 0.02\ s)$ of the ensemble for Φ = 3 vol % can decay asymptotically like an exponential function (Supporting Information). These results corroborated the success of using the CTRW framework to explain the exponential decay.

Note that the Barkai and Burov theory[40,74] cannot be directly employed to model polymer diffusion in nanocomposites because there are many Brownian trajectories, especially for the cases of Φ = 1.5 vol %. Moreover, the experiment has a fixed temporal resolution of 0.02 s. The adsorption and desorption events that occur at a time scale shorter than 0.02 s cannot be identified. But these events can still influence $P(x, t)$ at a time scale comparable to or longer than 0.02 s. Therefore, the trajectories may look Brownian but still exhibit an exponential decay of $P(x, t)$. To consider these factors, we modified the Barkai and Burov theory[40,74] by adding a component of the Gaussian process. We found that the modified approach is consistent with the experimental results when only varying the proportion of the Brownian trajectories, *i.e.*, the value of f in eq 11. This consistency indicates that even if only a portion of the trajectories obey the CTRW statistics, the tails of $P(x, t)$ can be asymptotically represented as exponential decay. This is expected from the CTRW theory, since the simply diffusing particles contribute

https://doi.org/10.1021/acsnano.3c06897
ACS Nano 2023, 17, 21708−21718

only Gaussian decay to $P(x, t)$. The exponential contribution diminishes this Gaussian decay due to switches between immobilization and mobility.

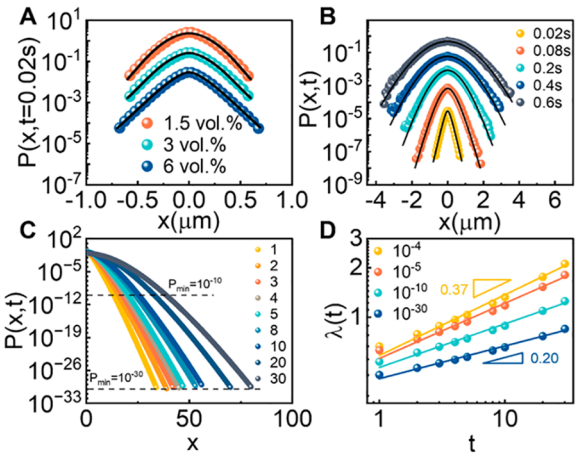

Figure 3. Theoretical results and their comparison with experimental data. (A) $P(x, t)$ of trajectories in mixtures with different Φ at t = 0.02 s. (B) $P(x, t)$ for data of Φ = 6 vol % at different t. The symbols represent the experimental results that removed the immobile trajectories, and the lines are the theoretical calculations according to eq 11. These curves are vertically shifted. (C) $P(x, t)$ of a CTRW process at different t. (D) $\lambda(t)$ *vs* t when using different P_{min} values as the cutoff for the CTRW process in (C).[54]

Microscopic Interpretation. We combined experiments, simulations, and theoretical approaches to show that adsorption-induced trapping can be used to trigger a gradual Gaussian-to-exponential transition of $P(x, t)$ in polymer nanocomposites. This occurs at a time scale much longer than the relaxation time t_d of the entangled polymers. We calculated various properties of the entangled polymer solution studied here. For example, the critical entanglement concentration of PEG (with molecular weight M_w = 40 kg/mol) is calculated according to $\Phi_e = (M_e/M_w)^{0.76} \approx 10$ vol %, where M_e = 2 kg/mol is the critical entanglement molecular weight. Therefore, the entangled polymer solution can be obtained by adding 40 kg/mol of PEG with a volume fraction of 20%. According to the tube theory, the reptation relaxation time is estimated by $t_d = 3N^3b^2/W\pi^2d^2$, where N is the number of segments (44 g/mol), $b \approx 0.58$ nm is the segmental length of PEG, d is the tube diameter, and $W = 3k_BT/b^2\zeta$ is the elementary Rouse rate with monomeric friction coefficient ζ.[61] We did not accurately know the value of ζ of 40 kg/mol PEG at T = 300 K. But we found $\zeta = 0.911 \times 10^{-15}$ kg/s for 81 kg/mol PEG at 360 K.[75] Using the well-known Williams–Landel–Ferry (WLF) equation, $\log(\alpha_T) = -C_1(T - T_0)/(C_2 + (T - T_0))$, where $\alpha_T = (\zeta(T)T_0)/(\zeta(T_0)T)$, C_1 = 2.306, and C_2 = 179.69 (at the reference temperature, T_0 = 348 K) are shifting constants.[59] Taken together, the calculation yields t_d = 79.2 ms for 81 kg/mol PEG melt at 300 K. Knowing that $\tau_d \sim N^{3.4}$ and $\tau_d \sim \Phi^{3(1-\nu)/(3\nu-1)}$ (ν = 0.588), the corresponding terminal relaxation time for 20 vol % 40 kg/mol PEG solution at 300 K was then estimated to be t_d = 0.57 ms, which is consistent with a simple estimation *via* the relation $t_d = R^2/D$, where D is the diffusion coefficient in the viscous regime and R is the polymer chain size. Note that the addition of nanoparticles may lead to an increase in relaxation time.[76] For example, $t_d = R^2/D$ = 1.1 ms was obtained using D of tracer polymers in mixtures with 6 vol % nanoparticles. Therefore, the acquisition time t_a = 20 ms should ensure that the observed diffusion occurred in the Fickian regime even in the presence of 6 vol % nanoparticles. The properties were calculated and tabulated in Table S1.

In the past decade, noticeable interest has grown in studying the adsorption and desorption of polymer on a solid surface using fast scanning calorimetry, depth profiling, and single-molecule tracking.[58,77,78] We have demonstrated that a polymer diffused on a solid–liquid interface *via* a CTRW mechanism where immobile periods were punctuated by desorption.[8,79] Inspired by this scenario, the reversible adsorption of polymers to nanoparticles' surface in a polymer–nanoparticle mixture can be used to invoke trapping provided that the nanoparticles are sufficiently large relative to the polymer to be "immobile" at the time scale of polymer diffusion that we observed.[80] Indeed, studies revealed that polymers could reversibly adsorb on nanoparticles' surfaces to form a bound layer in polymer–nanoparticle mixtures.[54,76,77] The number of adsorption (trapping) events can be controlled by tuning the volume fraction of the attractive nanoparticles.

As mentioned above, adsorption-induced trapping could be considered a well-defined mechanism to execute the CTRW dynamics. Note that the trapping cannot be simply considered as two states that lead to a delta function corresponding to trapped states plus a Gaussian tail. This is because, in the process, a diffusing polymer adsorbed on a nanoparticle surface with an immobile time τ before desorption. As shown in Figure 1C, most of the τ values are very short; as a result, a polymer may undergo multiple immobilizations in an experimental observable time window (20 ms). Kinetic Monte Carlo simulation indicates that for Φ = 6 vol %, a polymer can experience 300 encounters on nanoparticles' surface in 20 ms, corresponding to, on average, 9 trapping events when P_i = 0.03.

The present experimental system allows us to address a controversial issue regarding the value of α for the power-law decay $\lambda(t) \sim t^{\alpha}$. Granick *et al.* found that the length scale $\lambda(t)$ evolves as $\lambda(t) \sim t^{1/2}$.[46] Here, we found α = 1/3, which is consistent with results in many complex experimental systems.[13,47−50] Note that Chaudhuri *et al.* proposed that increasing the window of analyzed data, which involves an extremely large sample, results in a theoretical modification of α.[51,52] However, in Figure 1G, we found a constant α on a limited length and time scale. Given the consistency between experiments and the CTRW process, we simulated a CTRW model (eq S16) to produce $P(x, t)$ (Figure 3C).[53] We found that when the minimum probability P_{min} of finding a particle at x at time t varies from 10^{-4} to 10^{-30}, the value of $\lambda(t)$ and its power-law scaling of $\lambda(t) \sim t^{\alpha}$ could be changed when greatly varying time and length scales (Figure 3D). Therefore, from a strictly mathematical viewpoint, at least for the CTRW model, $\lambda(t)$ is not a well-defined quantity. However, $P_{min} = 10^{-30}$ is experimentally inaccessible, and such small values cannot be found in real-world data. Therefore, a constant α obtained from a given system over a range of length and time scales is still possible.

There are two major classes of stochastic models that describe the exponential distribution $P(x, t)$: the CTRW model and the model associated with multiple independent Gaussian processes.[9,25,46] The length scale $\lambda(t)$ evolves as $\lambda(t) \sim t^{1/2}$ [9,46] can be attained if it is described by the convolution of multiple independent Gaussian processes.[9,46] This might refer to diffusing objects that exhibit multiple diffusion coefficients or

https://doi.org/10.1021/acsnano.3c06897
ACS Nano 2023, 17, 21708−21718

where independent diffusive processes pertain intermittently to the same diffusing object, *i.e.*, diffusing diffusivity.[25] The presence of multiple Gaussian processes may originate from the heterogeneity of the environment, in time or space or both. On the other hand, the length scale $\lambda(t) \sim t^{\alpha}$ where α is not equal to 1/2 and evolves with time and length scales can be attained if it is a CTRW dynamics (Figure1G). Therefore, the different values of α could denote distinct mechanisms underlying observed exponential $P(x, t)$. While $\alpha = 1/2$ indicates the presence of multiple Gaussian processes, $\alpha \neq 1/2$ and a changing α (albeit experimentally indetectable) with time and length scales reflect the CTRW dynamics. This is supported by both the single-molecule trajectories and numerical simulations (Figures 1G and 3D).

As mentioned at the beginning of the paper, many works have reported the appearance of exponential tails. The universality of the phenomenon raises the following question: how can it be controlled? For the widespread Gaussian diffusion, control parameters are routinely used to unravel basic mechanisms; for example, the dependence of D on the system's temperature can teach us whether we have an activated process or not. But when dealing with systems with exponential tails, a difficulty emerges since the center part of the density is Gaussian and the tails are exponential. Further, the whole structure of the density is evolving in time. Hence, a distinct transport coefficient, like the D for the Gaussian case, has yet to be identified. Our work provided a chemical knob that yields insight into the transition. The performed analysis of single-particle trajectories corroborates that the presence of the immobile phase is responsible for the emergence of the exponential-to-Gaussian transition. While this behavior can be appropriately modeled as a CTRW process, it also aligns with other popular models. For instance, it resembles periods of low diffusivity that change slowly in the diffusing diffusivity model[25] and periods of ultraslow diffusion in the inhomogeneous diffusivity model,[81] or the immobile phase in the mobile−immobile model.[71] This observation suggests that trapping-induced immobilization, occurring over varying length and time scales, could be a generic mechanism that triggers the exponential tail of $P(x, t)$. However, the underlying mechanism may differ from system to system, resulting in variation of $\lambda(t) \sim t^{\alpha}$.

Moreover, the fact that the transition from Gaussian to exponential behavior can be controlled motivates possibilities for applications.[5−17] For example, in the field of diffusion-limited reactions, the existence of exponential tails of $P(x, t)$ enormously facilitates the probability of a fast reaction compared to the Gaussian case. In the case of insulin secretion in β-cells, the likelihood of a fast reaction (*i.e.*, secretion) is the main parameter distinguishing between proper function and malfunction of the cells.[82]

CONCLUSIONS

In conclusion, we used single-molecule fluorescence tracking to study the diffusion of PEG in nanoparticle−polymer mixtures. We demonstrated the triggering of the Gaussian-to-exponential transition for the shape of $P(x, t)$ at the tail using a mechanism involving polymer trapping *via* the reversible adsorption to the nanoparticle surface. We find "knobs", namely, nanoparticle concentration and interaction that enable the change in the shape of $P(x, t)$ in a well-defined way. This provides a path for experimentalists to explore the Gaussian-to-exponential transition that is usually extremely difficult to observe and manipulate due to the short-time nature of this behavior that occurs at a nanoscale. Interestingly, we observed that the time-dependent length scale $\lambda(t)$ in exponential tails exhibits the apparent power law $\lambda(t) \sim t^{\alpha}$ with a constant $\alpha = 1/3$. We found that the PEG diffusion is consistent with a modified large deviation approach for a CTRW. The Monte Carlo simulations can reproduce the experimental observations by involving a microscopic model of polymer trapping *via* the reversible adsorption to the nanoparticle surface. Taking advantage of this well-defined system, we show that $\lambda(t) \sim t^{1/3}$ is experimentally reproducible and correct in a phenomenological sense. This implies that the intermittent hopping dynamics present in the CTRW are a key ingredient for the observed behavior. However, from a mathematical viewpoint, the fitted value of α depends on the length and time scales over which the fitting is made. Our findings provide a well-defined experimental model that presents perspectives for the Brownian yet non-Gaussian phenomenon, especially the experimentally reproducible yet mathematically extremely slowly evolving behavior of a power law description of length scale $\lambda(t) \sim t^{\alpha}$. In the future, it is worthwhile to continue studying adsorption-induced trapping in polymer nanocomposites or in proximity to solid surfaces under non-equilibrium and shear conditions.[83]

METHODS

Experimental System. The weight-average molecular weight M_w and polydispersity index of PEG are 40 kg/mol and 1.1, respectively. We labeled amino-terminated PEG with ATTO 647 to prepare the polymer tracer. The radius of silica nanoparticles is 90 nm, 1 order of magnitude greater than the hydrodynamic radius of 40 kg/mol PEG in aqueous solutions (9.3 nm) (Supporting Information). The aqueous mixture contained 20 vol % PEG, 0−6 vol % of nanoparticles, and a small amount of dye-labeled PEG (10^{-11}−10^{-10} M), resulting in a sufficiently sparse density (<0.05 molecule/μm^2) to facilitate single-molecule localization. The polymer−nanoparticle interaction is switched on and off at pH = 2 and 10, respectively. Small-angle X-ray scattering measurements were performed to characterize the dispersion of nanoparticles in the polymer solution (Figure S1). The result did not show evidence of aggregation. Variable-angle illumination epifluorescence microscopy was used with acquisition time t_a = 20 ms to record trajectories of tracer polymers in mixtures, similar to a recent study (Figure S7B).[84] Further details of the experimental systems can be found in the Supporting Information.

Materials and Sample Preparation. Amino-functionalized polyethylene glycol and hydroxyl-terminated PEG were purchased from NANOCS, USA. The weight-average molecular weight M_w and polydispersity index of PEG are 40 kg/mol and 1.1, respectively. The tracer polymer was prepared by labeling amino-functionalized PEG with ATTO 647 (ATTO-TEC GmbH). The silica nanoparticles with a radius of 90 nm were purchased from Shanghai Aichun Biotechnology Co., Ltd. Their radii are 1 order of magnitude greater than the hydrodynamic radius of 40 kg/mol PEG in aqueous solutions (9.3 nm). The aqueous mixture contained 20 vol % PEG, 0−6 vol % of nanoparticles, and a small amount of dye-labeled PEG (10^{-11}−10^{-10} M), resulting in a sufficiently sparse density (<0.05 molecule/μm^2) to facilitate single-molecule localization. To prepare the polymer−nanoparticle aqueous mixture, each ingredient was mixed in a beaker with stirring at a shaker rate of 150 rpm for 5 h and then sealed and placed in a dark environment for about 4 h. The mixtures were titrated to pH = 2 with 2 M sulfuric acid or pH 10 with 2 M sodium carbonate. The PEG can adsorb on the silica surface for pH < 7 because of the hydrogen bonding between the ether group of PEG and the hydroxyl group on the silica surface. Small-angle X-ray scattering measurements were performed to characterize the dispersion of nanoparticles in the polymer solution (Figure S1). The result did not show evidence of aggregation.

https://doi.org/10.1021/acsnano.3c06897
ACS Nano 2023, 17, 21708−21718

To study nanoparticle diffusion in the polymer solution, amino-functionalized silica nanoparticles with a radius of 90 nm were coated with rhodamine. A trace amount of nanoparticles was dispersed in PEG solution containing 0 and 6 vol % nonfluorescent silica nanoparticles.

Microscope and Analysis. The single-molecule fluorescence tracking was performed with an objective-based Nikon Ti2-E total internal reflection fluorescence microscope (TIRFM) in conjunction with a high numerical aperture (1.49) 100× oil immersion objective and a Nikon LU-N4 laser unit with a laser power density of 0.35 mW/cm^2. The variable-angle illumination was applied so that an inclined excitation laser was at an angle smaller than the critical angle of total internal reflection.[85] The depth of the field was about 4 μm. A cooled EMCCD camera (iXon DU897) operating at −70 °C was used to capture time sequences of images at the acquisition time t_a = 20 ms. We set the EMCCD gain to 300× at 10 MHz readouts. The ATTO 647 functionalized PEG was excited by a continuous-wave 640 nm OBIS-LX diode laser. The measurements were performed at 22 °C. For each measurement, more than 60 one-minute movies were continuously captured at multiple locations and taken on multiple days. The trajectory was strung together from the image sequences by using a custom-developed tracking algorithm.

Kinetic Monte Carlo Simulation Model. We modeled the polymer diffusion using kinetic Monte Carlo simulations by integrating the adsorption process to the minimal model framework of an obstructed diffusion process consistent with a recently proposed mobile−immobile model.[71] The PEG chains were treated as random walkers on the lattice, since the experiment studied polymer diffusion in its viscous flow regime. A modified 2D square lattice was designed to incorporate obstacles in the following way (Figure S5A). Each lattice site was equivalent to a 0.016 × 0.016 μm^2 area, and an obstacle was modeled as a square occupying 12 × 12 lattice sites. The obstacles were randomly distributed on the lattice with different area fractions. The tracer, a PEG chain with a hydrodynamic radius RH ≈ 9.3 nm, randomly occupied a lattice site. To mimic the experimental results, the tracers were divided into immobile polymers and mobile polymers, based on the experimentally measured immobile and mobile population fractions. If the lattice sites that were occupied by obstacles is defined as Ω, then the random walk, $x(t)$ is given by

$$\tilde{x}_{j+1} = \tilde{x}_j + \eta_j\sqrt{4D\Delta t} \tag{13a}$$

$$\tilde{x}'_{j+1} = \tilde{x}'_j + \eta_j\sqrt{4D'\Delta t} \tag{13b}$$

$$t_{j+1} = t_j + \Delta t$$

$$x_{j+1}(t_{j+1}) = \begin{cases} \tilde{x}_{j+1}, & \text{if } \tilde{x}_{j+1} \cap \Omega \neq \emptyset \\ \text{invalid}, & \text{if } \tilde{x}_{j+1} \cap \Omega = \emptyset \end{cases} \quad \text{rebound} \tag{13c}$$

$$x_{j+1}(t_{j+1}) = \begin{cases} \tilde{x}_{j+1}, & \text{if } \tilde{x}_{j+1} \cap \Omega = \emptyset \\ \tilde{x}'_{j+1}, & \text{if } \tilde{x}_{j+1} \cap \Omega \neq \emptyset \end{cases} \quad \text{fixing on NP} \tag{13d}$$

where $(4D\Delta t)^{0.5}$ is equal to the mesh size, Δt is the time interval, η_j is a random unit vector in one of the four Cartesian axis directions, and $\emptyset$ denotes the empty set. D and D' represent the diffusion coefficients of PEG and nanoparticles in bulk solution, respectively. The immobile polymers were fixed at the same lattice site for a given lifetime. The apparent position was determined by a Gaussian distributed noise function, $\exp(-r^2/l^2)$, with l = 0.03−0.05 μm due to experimental localization. The diffusion of the mobile polymer follows the regular Fick's law (eq 13a). Once the polymer moves to a lattice adjacent to an obstacle, a probability P_i was given to determine whether the PEG walker is immobile (adsorbed) (eqs 13c and 13d). Thus, P_i was defined as the probability that an obstacle would successfully capture a PEG walker. The duration of immobilization was sampled from the experimentally measured immobile time distribution $\psi(\tau) \sim \tau^{-\beta}$ for $t_b < \tau < t_e$, where t_b and t_e are the upper and lower limits of τ, respectively. During the immobile times, the noise-induced location uncertainty was again represented by a Gaussian function, as mentioned above. The detailed simulation parameters are given in Table S2.

ASSOCIATED CONTENT

Supporting Information

The Supporting Information is available free of charge at https://pubs.acs.org/doi/10.1021/acsnano.3c06897.

Additional figures and characterization of the dispersion of nanoparticles, experimental considerations and analysis, property of polymer solution, kinetic Monte Carlo simulation, estimation of exponential tails, removal of immobile trajectories, and theoretical analysis about the exponential tails (PDF)

AUTHOR INFORMATION

Corresponding Author

Dapeng Wang − *State Key Laboratory of Polymer Physics and Chemistry, Changchun Institute of Applied Chemistry, Chinese Academy of Sciences, Changchun, Jilin 130022, People's Republic of China; University of Science and Technology of China, Hefei, Anhui 230026, People's Republic of China;* orcid.org/0000-0003-0276-7152; Email: wdp@ciac.ac.cn

Authors

Ming Hu − *State Key Laboratory of Polymer Physics and Chemistry, Changchun Institute of Applied Chemistry, Chinese Academy of Sciences, Changchun, Jilin 130022, People's Republic of China; University of Science and Technology of China, Hefei, Anhui 230026, People's Republic of China*

Hongbo Chen − *State Key Laboratory of Polymer Physics and Chemistry, Changchun Institute of Applied Chemistry, Chinese Academy of Sciences, Changchun, Jilin 130022, People's Republic of China*

Hongru Wang − *State Key Laboratory of Polymer Physics and Chemistry, Changchun Institute of Applied Chemistry, Chinese Academy of Sciences, Changchun, Jilin 130022, People's Republic of China; University of Science and Technology of China, Hefei, Anhui 230026, People's Republic of China*

Stanislav Burov − *Department of Physics, Institute of Nanotechnology and Advanced Materials, Bar-Ilan University, Ramat-Gan 52900, Israel*

Eli Barkai − *Department of Physics, Institute of Nanotechnology and Advanced Materials, Bar-Ilan University, Ramat-Gan 52900, Israel*

Complete contact information is available at: https://pubs.acs.org/10.1021/acsnano.3c06897

Author Contributions

‖M.H. and H.C. contributed equally to this work.

Author Contributions

The manuscript was written through contributions of all authors. All authors have given approval to the final version of the manuscript.

Notes

The authors declare no competing financial interest.

https://doi.org/10.1021/acsnano.3c06897
ACS Nano 2023, 17, 21708−21718

ACKNOWLEDGMENTS

We acknowledge financial support from the National Natural Science Foundation of China (Nos. 22073091 and 21873094), the National Key Research and Development Program of China (Nos. 2021YFC2101700 and 2021YFF0306400), the Youth Growth Science and Technology Program of Jilin Province (No. 20220508023RC), the Key Research Program of Frontier Sciences, Chinese Academy of Sciences (No. ZDBSLY-SLH033), and Israel Science Foundation grants (Nos. 1614/21 and 2796/20).

REFERENCES

(1) Metzler, R.; Jeon, J.-H.; Cherstvy, A. G.; Barkai, E. Anomalous Diffusion Models and Their Properties: Non-Stationarity, Non-Ergodicity, and Ageing at the Centenary of Single Particle Tracking. *Phys. Chem. Chem. Phys.* **2014**, *16*, 24128−24164.
(2) Kegel, W. K.; van Blaaderen, A. Direct Observation of Dynamical Heterogeneities in Colloidal Hard-Sphere Suspensions. *Science* **2000**, *287*, 290−293.
(3) Weeks, E. R.; Crocker, J. C.; Levitt, A. C.; Schofield, A.; Weitz, D. A. Three-Dimensional Direct Imaging of Structural Relaxation Near the Colloidal Glass Transition. *Science* **2000**, *287*, 627−631.
(4) Chaudhuri, P.; Berthier, L.; Kob, W. Universal Nature of Particle Displacements Close to Glass and Jamming Transitions. *Phys. Rev. Lett.* **2007**, *99*, No. 060604.
(5) Moringo, N. A.; Bishop, L. D. C.; Shen, H.; Misiura, A.; Carrejo, N. C.; Baiyasi, R.; Wang, W.; Ye, F.; Robinson, J. T.; Landes, C. F. A Mechanistic Examination of Salting out in Protein−Polymer Membrane Interactions. *Proc. Natl. Acad. Sci. U.S.A.* **2019**, *116*, 22938−22945.
(6) Yu, C.; Guan, J.; Chen, K.; Bae, S. C.; Granick, S. Single-Molecule Observation of Long Jumps in Polymer Adsorption. *ACS Nano* **2013**, *7*, 9735−9742.
(7) Skaug, M. J.; Mabry, J.; Schwartz, D. K. Intermittent Molecular Hopping at the Solid-Liquid Interface. *Phys. Rev. Lett.* **2013**, *110*, 256101.
(8) Wang, D.; He, C.; Stoykovich, M. P.; Schwartz, D. K. Nanoscale Topography Influences Polymer Surface Diffusion. *ACS Nano* **2015**, *9*, 1656−1664.
(9) Wang, B.; Anthony, S. M.; Bae, S. C.; Granick, S. Anomalous yet Brownian. *Proc. Natl. Acad. Sci. U.S.A.* **2009**, *106*, 15160−15164.
(10) Xue, C.; Zheng, X.; Chen, K.; Tian, Y.; Hu, G. Probing Non-Gaussianity in Confined Diffusion of Nanoparticles. *J. Phys. Chem. Lett.* **2016**, *7*, 514−519.
(11) Chen, P.; Yue, H.; Zhai, X.; Huang, Z.; Ma, G.-H.; Wei, W.; Yan, L.-T. Transport of a Graphene Nanosheet Sandwiched inside Cell Membranes. *Sci. Adv.* **2019**, *5*, No. eaaw3192.
(12) He, W.; Song, H.; Su, Y.; Geng, L.; Ackerson, B. J.; Peng, H. B.; Tong, P. Dynamic Heterogeneity and Non-Gaussian Statistics for Acetylcholine Receptors on Live Cell Membrane. *Nat. Commun.* **2016**, *7*, 11701.
(13) Åberg, C.; Poolman, B. Glass-like Characteristics of Intracellular Motion in Human Cells. *Biophys. J.* **2021**, *120*, 2355−2366.
(14) Leptos, K. C.; Guasto, J. S.; Gollub, J. P.; Pesci, A. I.; Goldstein, R. E. Dynamics of Enhanced Tracer Diffusion in Suspensions of Swimming Eukaryotic Microorganisms. *Phys. Rev. Lett.* **2009**, *103*, 198103.
(15) Babayekhorasani, F.; Dunstan, D. E.; Krishnamoorti, R.; Conrad, J. C. Nanoparticle Diffusion in Crowded and Confined Media. *Soft Matter* **2016**, *12*, 8407−8416.
(16) Höfling, F.; Franosch, T. Anomalous Transport in the Crowded World of Biological Cells. *Rep. Prog. Phys.* **2013**, *76*, No. 046602.
(17) Chakraborty, I.; Roichman, Y. Disorder-Induced Fickian, yet Non-Gaussian Diffusion in Heterogeneous Media. *Phys. Rev. Res.* **2020**, *2*, No. 022020.
(18) Silva, A. C.; Prange, R. E.; Yakovenko, V. M. Exponential Distribution of Financial Returns at Mesoscopic Time Lags: A New Stylized Fact. *Phys. A* **2004**, *344*, 227−235.
(19) Yamamoto, E.; Akimoto, T.; Kalli, A. C.; Yasuoka, K.; Sansom, M. S. P. Dynamic Interactions between a Membrane Binding Protein and Lipids Induce Fluctuating Diffusivity. *Sci. Adv.* **2017**, *3*, No. e1601871.
(20) Lanoiselée, Y.; Grebenkov, D. S. A Model of Non-Gaussian Diffusion in Heterogeneous Media. *J. Phys. A Math. Theor.* **2018**, *51*, 145602.
(21) Miyaguchi, T.; Akimoto, T.; Yamamoto, E. Langevin Equation with Fluctuating Diffusivity: A Two-State Model. *Phys. Rev. E* **2016**, *94*, No. 012109.
(22) Jain, R.; Sebastian, K. L. Diffusion in a Crowded, Rearranging Environment. *J. Phys. Chem. B* **2016**, *120*, 3988−3992.
(23) Sposini, V.; Chechkin, A. V.; Seno, F.; Pagnini, G.; Metzler, R. Random Diffusivity from Stochastic Equations: Comparison of Two Models for Brownian yet Non-Gaussian Diffusion. *New J. Phys.* **2018**, *20*, No. 043044.
(24) Hidalgo-Soria, M.; Barkai, E.; Burov, S. Cusp of Non-Gaussian Density of Particles for a Diffusing Diffusivity Model. *Entropy* **2021**, *23*, 231.
(25) Chubynsky, M. V.; Slater, G. W. Diffusing Diffusivity: A Model for Anomalous, yet Brownian. *Diffusion. Phys. Rev. Lett.* **2014**, *113*, No. 098302.
(26) Ślęzak, J.; Metzler, R.; Magdziarz, M. Superstatistical Generalised Langevin Equation: Non-Gaussian Viscoelastic Anomalous Diffusion. *New J. Phys.* **2018**, *20*, No. 023026.
(27) Chechkin, A. V.; Seno, F.; Metzler, R.; Sokolov, I. M. Brownian yet Non-Gaussian Diffusion: From Superstatistics to Subordination of Diffusing Diffusivities. *Phys. Rev. X* **2017**, *7*, No. 021002.
(28) Postnikov, E. B.; Chechkin, A.; Sokolov, I. M. Brownian yet Non-Gaussian Diffusion in Heterogeneous Media: From Superstatistics to Homogenization. *New J. Phys.* **2020**, *22*, No. 063046.
(29) Burov, S.; Barkai, E. Time Transformation for Random Walks in the Quenched Trap Model. *Phys. Rev. Lett.* **2011**, *106*, 140602.
(30) Burov, S.; Barkai, E. Occupation Time Statistics in the Quenched Trap Model. *Phys. Rev. Lett.* **2007**, *98*, 250601.
(31) Akimoto, T.; Barkai, E.; Saito, K. Non-Self-Averaging Behaviors and Ergodicity in Quenched Trap Models with Finite System Sizes. *Phys. Rev. E* **2018**, *97*, No. 052143.
(32) Baldovin, F.; Orlandini, E.; Seno, F. Polymerization Induces Non-Gaussian Diffusion. *Front. Phys.* **2019**, *7*, 124.
(33) Hidalgo-Soria, M.; Barkai, E. Hitchhiker Model for Laplace Diffusion Processes. *Phys. Rev. E* **2020**, *102*, No. 012109.
(34) Yin, Q.; Li, Y.; Marchesoni, F.; Nayak, S.; Ghosh, P. K. Non-Gaussian Normal Diffusion in Low Dimensional Systems. *Front. Phys.* **2021**, *16*, 33203.
(35) Montroll, E. W.; Weiss, G. H. Random Walks on Lattices. II. *J. Math. Phys.* **1965**, *6*, 167−181.
(36) Haus, J. W.; Kehr, K. W. Diffusion in Regular and Disordered Lattices. *Phys. Rep.* **1987**, *150*, 263−406.
(37) Dai, L.-J.; Fu, C.-L.; Zhu, Y.-L.; Li, Z.-W.; Sun, Z.-Y. Probing Intermittent Motion of Polymer Chains in Weakly Attractive Nanocomposites. *Chin. J. Polym. Sci.* **2020**, *38*, 620−628.
(38) Metzler, R.; Klafter, J. The Random Walk's Guide to Anomalous Diffusion: A Fractional Dynamics Approach. *Phys. Rep.* **2000**, *339*, 1−77.
(39) Wang, W.; Barkai, E.; Burov, S. Large Deviations for Continuous Time Random Walks. *Entropy* **2020**, *22*, 697.
(40) Barkai, E.; Burov, S. Packets of Diffusing Particles Exhibit Universal Exponential Tails. *Phys. Rev. Lett.* **2020**, *124*, No. 060603.
(41) Lanoiselée, Y.; Moutal, N.; Grebenkov, D. S. Diffusion-Limited Reactions in Dynamic Heterogeneous Media. *Nat. Commun.* **2018**, *9*, 4398.
(42) Monserud, J. H.; Schwartz, D. K. Interfacial Molecular Searching Using Forager Dynamics. *Phys. Rev. Lett.* **2016**, *116*, No. 098303.

https://doi.org/10.1021/acsnano.3c06897
ACS Nano 2023, 17, 21708−21718

(43) Xue, C.; Shi, X.; Tian, Y.; Zheng, X.; Hu, G. Diffusion of Nanoparticles with Activated Hopping in Crowded Polymer Solutions. *Nano Lett.* **2020**, *20*, 3895−3904.
(44) Dai, X.; Zhu, Z.; Li, Y.; Yang, B.; Xu, J.-F.; Dong, Y.; Zhou, X.; Yan, L.-T.; Liu, D. Shutter" Effects Enhance Protein Diffusion in Dynamic and Rigid Molecular Networks. *J. Am. Chem. Soc.* **2022**, *144*, 19017−19025.
(45) Wagner, C. E.; Turner, B. S.; Rubinstein, M.; McKinley, G. H.; Ribbeck, K. A Rheological Study of the Association and Dynamics of MUC5AC Gels. *Biomacromolecules* **2017**, *18*, 3654−3664.
(46) Wang, B.; Kuo, J.; Bae, S. C.; Granick, S. When Brownian Diffusion Is Not Gaussian. *Nat. Mater.* **2012**, *11*, 481−485.
(47) Miotto, J. M.; Pigolotti, S.; Chechkin, A. V.; Roldán-Vargas, S. Length Scales in Brownian yet Non-Gaussian Dynamics. *Phys. Rev. X* **2021**, *11*, No. 031002.
(48) Rusciano, F.; Pastore, R.; Greco, F. Fickian Non-Gaussian Diffusion in Glass-Forming Liquids. *Phys. Rev. Lett.* **2022**, *128*, 168001.
(49) Lee, C. H.; Crosby, A. J.; Emrick, T.; Hayward, R. C. Characterization of Heterogeneous Polyacrylamide Hydrogels by Tracking of Single Quantum Dots. *Macromolecules* **2014**, *47*, 741−749.
(50) Garamella, J.; Regan, K.; Aguirre, G.; McGorty, R. J.; Robertson-Anderson, R. M. Anomalous and Heterogeneous DNA Transport in Biomimetic Cytoskeleton Networks. *Soft Matter* **2020**, *16*, 6344−6353.
(51) Chaudhuri, P.; Gao, Y.; Berthier, L.; Kilfoil, M.; Kob, W. A Random Walk Description of the Heterogeneous Glassy Dynamics of Attracting Colloids. *J. Phys.: Condens. Matter* **2008**, *20*, 244126.
(52) Berthier, L.; Flenner, E.; Szamel, G. Are Supercooled Liquids Fickian yet Non Gaussian? 2022. arXiv:2210.07119.
(53) Rusciano, F.; Pastore, R.; Greco, F. Supercooled Liquids Are Fickian yet Non-Gaussian. 2022. arXiv:2212.09679.
(54) Jimenez, A. M.; Zhao, D.; Misquitta, K.; Jestin, J.; Kumar, S. K. Exchange Lifetimes of the Bound Polymer Layer on Silica Nanoparticles. *ACS Macro Lett.* **2019**, *8*, 166−171.
(55) Asgari, N.; Baaske, M. D.; Orrit, M. Burst-by-Burst Measurement of Rotational Diffusion at Nanosecond Resolution Reveals Hot-Brownian Motion and Single-Chain Binding. *ACS Nano* **2023**, *17*, 12684−12692.
(56) Van Hove, L. Correlations in Space and Time and Born Approximation Scattering in Systems of Interacting Particles. *Phys. Rev.* **1954**, *95*, 249−262.
(57) Choi, J.; Hore, M. J. A.; Meth, J. S.; Clarke, N.; Winey, K. I.; Composto, R. J. Universal Scaling of Polymer Diffusion in Nanocomposites. *ACS Macro Lett.* **2013**, *2*, 485−490.
(58) Bailey, E. J.; Winey, K. I. Dynamics of Polymer Segments, Polymer Chains, and Nanoparticles in Polymer Nanocomposite Melts: A Review. *Prog. Polym. Sci.* **2020**, *105*, 101242.
(59) Lin, C.-C.; Gam, S.; Meth, J. S.; Clarke, N.; Winey, K. I.; Composto, R. J. Do Attractive Polymer−Nanoparticle Interactions Retard Polymer Diffusion in Nanocomposites? *Macromolecules* **2013**, *46*, 4502−4509.
(60) Ge, T.; Kalathi, J. T.; Halverson, J. D.; Grest, G. S.; Rubinstein, M. Nanoparticle Motion in Entangled Melts of Linear and Nonconcatenated Ring Polymers. *Macromolecules* **2017**, *50*, 1749−1754.
(61) Zamponi, M.; Kruteva, M.; Monkenbusch, M.; Willner, L.; Wischnewski, A.; Hoffmann, I.; Richter, D. Cooperative Chain Dynamics of Tracer Chains in Highly Entangled Polyethylene Melts. *Phys. Rev. Lett.* **2021**, *126*, 187801.
(62) Cai, L.-H.; Panyukov, S.; Rubinstein, M. Hopping Diffusion of Nanoparticles in Polymer Matrices. *Macromolecules* **2015**, *48*, 847−862.
(63) Park, J.; Bailey, E. J.; Composto, R. J.; Winey, K. I. Single-Particle Tracking of Nonsticky and Sticky Nanoparticles in Polymer Melts. *Macromolecules* **2020**, *53*, 3933−3939.
(64) Wong, I. Y.; Gardel, M. L.; Reichman, D. R.; Weeks, E. R.; Valentine, M. T.; Bausch, A. R.; Weitz, D. A. Anomalous Diffusion Probes Microstructure Dynamics of Entangled F-Actin Networks. *Phys. Rev. Lett.* **2004**, *92*, 178101.
(65) Sabri, A.; Xu, X.; Krapf, D.; Weiss, M. Elucidating the Origin of Heterogeneous Anomalous Diffusion in the Cytoplasm of Mammalian Cells. *Phys. Rev. Lett.* **2020**, *125*, No. 058101.
(66) Jeon, J.-H.; Javanainen, M.; Martinez-Seara, H.; Metzler, R.; Vattulainen, I. Protein Crowding in Lipid Bilayers Gives Rise to Non-Gaussian Anomalous Lateral Diffusion of Phospholipids and Proteins. *Phys. Rev. X* **2016**, *6*, No. 021006.
(67) Simavilla, D. N.; Huang, W.; Vandestrick, P.; Ryckaert, J.-P.; Sferrazza, M.; Napolitano, S. Mechanisms of Polymer Adsorption onto Solid Substrates. *ACS Macro Lett.* **2017**, *6*, 975−979.
(68) Burov, S.; Tabei, S. M. A.; Huynh, T.; Murrell, M. P.; Philipson, L. H.; Rice, S. A.; Gardel, M. L.; Scherer, N. F.; Dinner, A. R. Distribution of Directional Change as a Signature of Complex Dynamics. *Proc. Natl. Acad. Sci. U.S.A.* **2013**, *110*, 19689−19694.
(69) Lin, C.-C.; Parrish, E.; Composto, R. J. Macromolecule and Particle Dynamics in Confined Media. *Macromolecules* **2016**, *49*, 5755−5772.
(70) Meth, J. S.; Gam, S.; Choi, J.; Lin, C.-C.; Composto, R. J.; Winey, K. I. Excluded Volume Model for the Reduction of Polymer Diffusion into Nanocomposites. *J. Phys. Chem. B* **2013**, *117*, 15675−15683.
(71) Doerries, T. J.; Chechkin, A. V.; Schumer, R.; Metzler, R. Rate Equations, Spatial Moments, and Concentration Profiles for Mobile-Immobile Models with Power-Law and Mixed Waiting Time Distributions. *Phys. Rev. E* **2022**, *105*, No. 014105.
(72) Koga, T.; Barkley, D.; Nagao, M.; Taniguchi, T.; Carrillo, J.-M. Y.; Sumpter, B. G.; Masui, T.; Kishimoto, H.; Koga, M.; Rudick, J. G.; Endoh, M. K. Interphase Structures and Dynamics near Nanofiller Surfaces in Polymer Solutions. *Macromolecules* **2018**, *51*, 9462−9470.
(73) Senses, E.; Narayanan, S.; Faraone, A. Nanoscale Particle Motion Reveals Polymer Mobility Gradient in Nanocomposites. *ACS Macro Lett.* **2019**, *8*, 558−562.
(74) Korabel, N.; Barkai, E. Paradoxes of Subdiffusive Infiltration in Disordered Systems. *Phys. Rev. Lett.* **2010**, *104*, 170603.
(75) Niedzwiedz, K.; Wischnewski, A.; Pyckhout-Hintzen, W.; Allgaier, J.; Richter, D.; Faraone, A. Chain Dynamics and Viscoelastic Properties of Poly(Ethylene Oxide). *Macromolecules* **2008**, *41*, 4866−4872.
(76) Bailey, E. J.; Griffin, P. J.; Composto, R. J.; Winey, K. I. Characterizing the Areal Density and Desorption Kinetics of Physically Adsorbed Polymer in Polymer Nanocomposite Melts. *Macromolecules* **2020**, *53*, 2744−2753.
(77) Monnier, X.; Napolitano, S.; Cangialosi, D. Direct Observation of Desorption of a Melt of Long Polymer Chains. *Nat. Commun.* **2020**, *11*, 4354.
(78) Niu, Q.; Wang, D. Probing the Polymer Anomalous Dynamics at Solid/Liquid Interfaces at the Single-Molecule Level. *Curr. Opin. Colloid Interface Sci.* **2019**, *39*, 162−172.
(79) Wang, D.; Wu, H.; Schwartz, D. K. Three-Dimensional Tracking of Interfacial Hopping Diffusion. *Phys. Rev. Lett.* **2017**, *119*, 268001.
(80) Kumar, S. K.; Ganesan, V.; Riggleman, R. A. Perspective: Outstanding Theoretical Questions in Polymer-Nanoparticle Hybrids. *J. Chem. Phys.* **2017**, *147*, No. 020901.
(81) Massignan, P.; Manzo, C.; Torreno-Pina, J. A.; García-Parajo, M. F.; Lewenstein, M.; Lapeyre, G. J. Nonergodic Subdiffusion from Brownian Motion in an Inhomogeneous Medium. *Phys. Rev. Lett.* **2014**, *112*, 150603.
(82) Tabei, S. M. A.; Burov, S.; Kim, H. Y.; Kuznetsov, A.; Huynh, T.; Jureller, J.; Philipson, L. H.; Dinner, A. R.; Scherer, N. F. Intracellular Transport of Insulin Granules Is a Subordinated Random Walk. *Proc. Natl. Acad. Sci. U.S.A.* **2013**, *110*, 4911−4916.
(83) Peng, B.; Yang, Z.; Yang, L.; Chen, J.; Liu, L.; Wang, D. Reducing the Solvent Quality Gives Rise to the Outward Migration of a Star Polymer in Poiseuille Flow. *Macromolecules* **2022**, *55*, 3396−3407.

https://doi.org/10.1021/acsnano.3c06897
ACS Nano 2023, 17, 21708−21718

(84) Zhang, Z.; Chen, H.; Hu, M.; Wang, D. Single-Molecule Tracking of Reagent Diffusion during Chemical Reactions. *J. Am. Chem. Soc.* **2023**, *145*, 10512−10521.
(85) Wang, D.; Agrawal, A.; Piestun, R.; Schwartz, D. K. Enhanced Information Content for Three-Dimensional Localization and Tracking Using the Double-Helix Point Spread Function with Variable-Angle Illumination Epifluorescence Microscopy. *Appl. Phys. Lett.* **2017**, *110*, 211107.

https://doi.org/10.1021/acsnano.3c06897
ACS Nano 2023, 17, 21708−21718